Geometry of Braided DNA Dictates Supercoiling Partitioning

Yifeng Hong[1,#], Gundeep Singh[2,#], Hanjie Wang[3,#], Seong ha Park[3,4,#], and Michelle D. Wang[3,4,*]

[1]Department of Electrical and Computer Engineering, Cornell University, Ithaca, NY 14853, USA

[2]Biophysics Program, Cornell University, Ithaca, NY 14853, USA

[3]Department of Physics & LASSP, Cornell University, Ithaca, NY 14853, USA

[4]Howard Hughes Medical Institute, Cornell University, Ithaca, NY 14853, USA

[#]These authors contributed equally

*Correspondence: mwang@physics.cornell.edu

DNA's helical structure requires the replisome to rotate relative to parental DNA during replication, generating supercoiling that partitions ahead and behind the fork. The influence of DNA substrate geometry on supercoiling partitioning and torsional resistance remains unclear. Here, we engineered DNA-braiding substrates with end separations found during replication, measured braiding torques using an angular optical trap, and interpreted the results using Monte Carlo simulations. A substrate with small separations readily initiated braiding, suggesting that the fork would rotate during replication, partitioning supercoiling behind the replisome and reducing torsional resistance. In contrast, a substrate with a substantial separation at one end imposed a pronounced 'torsional barrier' that hindered braiding initiation, suggesting a lack of fork rotation during replication, so supercoiling would partition ahead of the replisome. Our findings reveal a physical mechanism in which daughter-DNA geometry could modulate replisome dynamics, manage topological stress, and regulate replication progression *in vivo*.

Introduction

During DNA replication, a replisome duplicates the parental DNA into two daughter strands. Because of DNA's helical structure, a progressing replisome must track the DNA helical groove via rotation relative to the DNA substrate (*1–5*). This rotation can potentially intertwine the two daughter strands and thereby prevent chromosome segregation during mitosis (*3*, *6–12*). In addition, DNA replication inherently creates torsional stress that, in turn, hinders the progression of the replisome (*1*, *3–5*, *13*). *In vivo*, these difficulties are partially relieved by the action of topoisomerases. Although topoisomerases are essential in relaxing torsional stress (*2*, *14*, *15*), they cannot always keep up with replication (*11*, *16–23*). Therefore, daughter-strand intertwining and torsional stress accumulation can occur during replication elongation, especially as the replisome approaches termination (*7–10*, *24*, *25*). Despite this problem being inherent to replication, we have a limited understanding of the mechanics governing supercoiling partitioning to the daughter strands and daughter-strand intertwining (also referred to as braiding), as well as the extent of torsional stress the replisome experiences.

Previously, we hypothesized that this problem is inherently dictated by the torsional mechanical properties of the single- and double-DNA substrates (*4*). Because torque must be balanced at the replisome, supercoiling partitioning between the front and back of the replisome is solely determined by the torsional resistance of twisting the single-DNA substrate in front of the replisome and the torsional resistance of braiding the double-DNA substrate behind the replisome. The torsional resistance to braiding double-DNA substrate is expected to critically depend on the separation between the two DNA molecules at each end (*26*, *27*). *In vivo*, the end separation of the two daughter strands at the replisome might be relatively small, on the order of 20-50 nm, as estimated by the size of the replisome (*4*, *28*). At the end distal to the replisome where the two daughter DNA molecules extend away from the fork, the separation may increase significantly until structural maintenance of chromosomes (SMC) proteins bring the two strands together to a distance of about 35 nm (*29–31*). Thus, elucidating how daughter-strand geometry affects DNA supercoiling partitioning requires direct torque

measurements of braiding DNA substrates with defined end separations (20-50 nm). This measurement feat has not been previously attainable.

Previous single-molecule studies selected braids among DNA tethers anchored to surfaces at random locations (*4*, *26*, *32–45*) and estimated the anchor separation by assuming the separations at both ends were identical (*4*, *26*, *32–35*, *38*, *45*). However, it is very challenging to identify a braid with an end separation < 100 nm, and the equal-separation assumption likely does not hold for most surface-tethered DNA braids. Experiments using multiple optical traps can control the geometry of the two DNA molecules while braiding (*46*, *47*), but the micron-sized dimensions of the trapping particles limit the DNA end separations to large values. Furthermore, although knowledge of the torque to braid DNA is essential, direct torque measurements are lacking in most previous experimental studies.

In this work, we engineered a DNA braiding substrate with an anchor separation of about 24 nm at both ends to better mimic the *in vivo* geometry, along with two other braiding substrates with larger anchor separations for comparison. Using the angular optical trap (AOT), we directly measured the torque required to braid these substrates. Our measurements provided the torque required to initiate the braiding, the torsional stiffness of braided DNA, and the torque needed to buckle a DNA braid into a plectoneme. To better understand how braiding geometry governs the torsional mechanics of braiding, we performed Monte Carlo (MC) simulations to facilitate the interpretation of our experimental results. The framework laid out in this work should provide insights into how braiding geometry impacts replication-generated torsional stress and the extent of the daughter-strand intertwining during replication.

Results

Engineered DNA Braiding Substrates with Defined Geometries

To study DNA braiding under well-defined geometries, we developed methods to engineer two DNA braiding substrates (Methods), namely the ‘O substrate’ (Fig. 1a) and the ‘V

substrate' (Fig. 1b). Each substrate was constructed from a customized plasmid (Methods) and contains two DNA segments of essentially identical lengths for braiding.

The 'O substrate' was designed with minimal separations at both ends (Fig. 1a; Methods). This design best mimics an *in vivo* configuration in which the two replicated DNA strands are held closely together at one end by the replisome and at the other end by SMC proteins. To construct this substrate, we created two ssDNA gaps (69 bp or 70 bp) symmetrically located at half a plasmid length apart, followed by filling in with multi-digoxigenin-labeled or multi-biotin-labeled nucleotides at the two sites. The final product thus has two distinct short surface-anchoring sites that define the end separations. These sites are also multi-tagged, enabling torsional constraint to either an anti-digoxigenin-coated or streptavidin-coated surface. In addition, each 'daughter' DNA strand was nicked (Methods), to mimic the *in vivo* configuration where both the leading and lagging strands are thought to be able to rotate around the DNA helical axis during replication (*1*, *2*, *4*).

The 'V substrate' was designed to have a minimal separation at one end while allowing the other end to have a greater separation (Fig. 1b; Methods). This design mimics an *in vivo* configuration where daughter strands are held closely together at one end by the replisome, but the other end might be further apart (e.g., when SMC proteins fail to bring the two strands together (*48*)). To construct this substrate, the plasmid was linearized and then ligated with a biotin-labeled adapter at each end for surface anchoring. A ssDNA gap was created in the middle of the template, resulting in a 70 bp region containing multi-digoxigenin-labeled nucleotides. Before measurements, each daughter strand in the 'V substrate' was nicked to prevent torsion accumulation within each 'daughter' DNA (Methods).

Upon surface immobilization between an anti-digoxigenin-coated quartz cylinder optically trapped with the AOT and a streptavidin-coated coverslip surface (Methods), the 'O substrate' has a minimal end separation at each end of the two 'daughter' DNA molecules (Fig. 1c, top). In contrast, the 'V substrate' has a minimal end separation at the quartz cylinder and a variable end separation at the coverslip surface. This variable separation can be substantial compared with the length of each 'daughter' DNA (Fig. 1c, middle).

For completeness, we also examined a braiding geometry with wide separations at both ends. We anchored individual 6.5 kb DNA molecules (Methods) at random locations on the coverslip surface and then selected a cylinder that was tethered via two DNA molecules (*4*). This substrate has substantial separations at both ends compared to the length of each 'daughter' DNA molecule (Fig. 1c, bottom). For convenience, we refer to this configuration as the 'U substrate'.

Braiding DNA with Minimal End Separations

The 'O substrate' has small anchor separations at both ends and should best resemble the *in vivo* geometry of daughter strands during replication. It has nearly identical end separations at both ends (a and b), which are significantly smaller than the length l of each 'daughter' DNA molecule ($a = b \ll l$) (Fig. 2a). To determine the torque required to braid the 'O substrate', we used the AOT, which allows simultaneous measurements of torque, rotational angle, force, and extension of DNA via a nanofabricated cylinder (*4*, *5*, *49–56*). Once torsionally constrained between the coverslip surface and the cylinder (Fig. 2a; Methods), the 'O substrate' was held at a constant force and braided via rotation of the cylinder. Thus, the number of turns added by the cylinder equals the catenation number (the number of times the two daughter strands intertwine each other).

Using the AOT, we measured the torque required to braid the 'O substrate' while simultaneously monitoring its corresponding extension (Fig. 2a). As turns are added, the torque increases due to resistance to braiding, and the extension decreases due to the two 'daughter' DNA molecules helically wrapping around each other to form a braided structure. When the braiding torque reaches a critical value, the torque plateaus while the extension shortens sharply, indicating buckling of the braided DNA to form a plectoneme. We found that the number of turns required to buckle a DNA braid increases with force. As more turns are added, the plectoneme of the braided DNA continues to extrude, indicated by a linear extension decrease. These behaviors are reminiscent of the torsional properties of the single-DNA substrate measured under the same conditions (Fig. 2b), consistent with the results from our previous studies (*4*, *49–59*).

We found that the extension-turns relation is essentially an even function, nearly symmetric about zero turn number, and the torque-turns relation is essentially an odd function, nearly antisymmetric about zero turn number. We detected some slight asymmetries (Fig. S1), likely due to helix-specific interactions (*60–64*). These predominately symmetric features suggest that the inherent chirality of DNA molecules does not play a significant role in the torsional mechanical properties of braiding. As our work aims to understand the supercoiling generation during replication, we focus on the torsional mechanics of the right-handed braid (R-braid), which corresponds to (+) supercoiling.

To more rigorously understand these braiding features, we performed MC simulations of the 'O substrate' (Fig. 2a) and the single-DNA substrate (Fig. 2b) (Methods; Table S1). This approach extended a previous simulation framework (*26*, *65*) by incorporating a Debye-Huckel electrostatic interaction potential and a more accurate sampling of topologies (Methods). These improvements enabled us to compute torsional mechanics over a broader range of catenation densities for braided conformations, including torque in the post-buckling regime, which has not been reported in previous MC simulations. We found that the simulated extension-turns and torque-turns relations under different forces agree well with measurements for the 'O substrate', providing validation of our simulation method. Notably, the previous MC simulation work on DNA braiding predicted a substantially steeper torque-turns relation under the same force (*26*) than our measurements.

We further analyzed the braiding data shown in Fig. 2a and found that both the measured and simulated torques increase linearly with turns near zero turns, albeit with a slight torque discontinuity due to small but non-zero end separations (Fig. 2a). As more turns are introduced, these torques exhibit some nonlinearity, indicating a twist-stiffening effect (Fig. S1a), as suggested by a previous theoretical study (*27*). To characterize the torsional resistance to braiding at a small number of turns, we determined the torsional stiffness of braiding using the slope of the torque-turns relation near zero turns (Methods). We then converted this stiffness to the effective twist persistence length C_{eff}, a parameter independent of the DNA length (*4*), and found it to be insensitive to tension over the range from 0.5 to 3 pN (Fig. 2c).

In comparison with the single-DNA substrate, the 'O substrate' has a C_{eff} about 4 to 5 times smaller (Fig. 2c), indicating that 'O substrate' is easier to twist. However, the 'O substrate' is more resistant to buckling, with buckling occurring at a higher torque and a larger superhelical density (Fig. 2d). Unlike the single-DNA substrate, the 'O substrate' extension slope also shows a non-monotonic force-dependent behavior after buckling (Fig. S2). These results from the 'O substrate' establish the torsional mechanical properties necessary to model supercoiling partitioning during DNA replication.

Braiding DNA with a Substantial End Separation

The 'V substrate' has one end with a small separation ($a \ll l$) and another with a substantially larger separation (b), mimicking a case where the replisome brings one end together, but SMC proteins fail to bring the other end together. The 'U substrate' has both ends separated by a substantial separation, a configuration that may not readily occur *in vivo*. We have included studies of the 'U substrate' for completeness and comparison with previous studies.

Using the AOT, we measured torque-turns and extension-turns relations of the 'V substrate' (Fig. 3a) and the 'U substrate' (Fig. 3b). The measured relations have some similarities with those measured with the 'O substrate' (Fig. 2a) but with significant differences. The most distinguishing features occur near zero turns (more precisely, between -0.5 turns and +0.5 turns). For both substrates, the torque discontinuity near zero turns, which we refer to as the 'torque gap' τ_{gap} (Methods), becomes more prominent (Fig. 3a,b). Beyond the zero turns before buckling, the extension decreases more steeply with turns, which we characterize by the 'hat-top slope', and the buckling occurs at a lower number of turns.

The U substrate has additional striking features within ±0.5 turns (Fig. 3b). We detected two torque overshoots: a positive overshoot centered around +0.25 turns and a negative overshoot centered around -0.25 turns. These overshoots can be one order of magnitude greater than the torque gap. Because the overshoots peak sharply above the smoother torque profile after the braiding initiates, we characterize their amplitude using the parameter 'torque overshoot' $\tau_{\mathrm{overshoot}}$. Concurrent with observed 'torque-overshoots' are sharp extension drops

from 0 to ±0.5 turns as the two 'daughter' DNA molecules are first brought in contact to initiate the braiding. We refer to this extension drop as the 'hat tip' $h_{\mathrm{hat_tip}}$, because the extension-turns relation is sometimes called a hat curve.

To estimate the geometries for the V substrate and the U substrate, we performed MC simulations with various combinations of a and b and identified those that best match the measurements. These simulation results indicate that the V substrate has a significant separation at only one end, while the U substrate has significant separations at both ends, consistent with the expected geometries of these templates. We will follow up in the section below with a more rigorous comparison of the measurements and simulations and provide detailed interpretations.

These torsional features of the 'V substrate' and 'U substrate' demonstrate that the geometry of the braiding substrates significantly alters the torsional mechanics of braiding. The significant torque gap represents a 'torsional barrier' to the initiation of braiding. The dramatic torque overshoot leads to a non-monotonic torque dependence on the DNA superhelical density, creating a 'kinetic torsional barrier' to braiding (Fig. S3); thus, even if braiding is thermodynamically favored, its onset can be delayed by the high barrier to initiation.

Modeling How Braiding Geometry Alters Torsional Mechanics

The torsional measurements from the 'V substrate' and 'U substrate' in Fig. 3 show that as the end separations increase, several features emerge and become significant. Most notable features include a torque overshoot, hat tip, torque gap, and hat-top slope, which are further clarified in Fig. 4a. Understanding how these torsional features depend on the braiding geometry requires theoretical guidance. Thus, we performed MC simulations to further explore the torsional properties of DNA braiding over a broader range of combinations of end separations a and b. For completeness, we also modified a previous geometric model (*26*) of braiding to account for braiding geometry with different separations at the two ends (Methods; Table S2).

Our simulations show that the hat tip and the torque overshoot, i.e., torsional properties within ±0.5 turns, are essentially proportional to the product $a \cdot b$ (Fig. 4b, left; Fig. S4a). To compare simulations with measurements, we examined the torque overshoot versus hat tip and found good agreement (Fig. 4c, left). Thus, these results reveal that a torque overshoot will occur only if both ends of a braiding substrate have a substantial separation. Consistent with this conclusion, we did not detect any torque overshoot when braiding the 'O substrate' (Fig. 2a) or the 'V substrate' (Fig. 3a), which have a minimal end separation at one end or both ends. In contrast, the 'U substrate' can have substantial end separations at both ends and readily yield a detectable torque overshoot (Fig. 3b). In addition, predictions from the modified geometric model are in reasonable agreement with both the simulations and measurements, indicating that this simple model can be used to interpret the torsional properties of braiding within ±0.5 turns before braiding initiates.

Our simulations also show that the hat-top slope magnitude and the torque gap, i.e., torsional properties at or beyond ±0.5 turns, increase monotonically with $a + b$ (Fig. 4b, right; Fig. S4b). We again compared simulations and measurements by examining the torque gap versus the hat-top slope magnitude and found them in good agreement (Fig. 4c, right). Thus, these results show that a torque gap will appear if at least one end of a braiding substrate has a substantial separation. Indeed, we detected a distinct torque gap when braiding either the 'V substrate' (Fig. 3a) or the 'U substrate' (Fig. 3b), while the torque gap of braiding the 'O substrate' was minimal (Fig. 2a). Importantly, predictions from the modified geometric model deviate significantly from both simulations and measurements. Thus, while this simple model works well before braiding initiates, it cannot be used to interpret torsional properties once braiding begins; therefore, we will not use it further in subsequent analysis. This highlights the need to rely on simulations for understanding the geometry-governed torsional properties of braiding.

We further examined how braiding geometry modulates the effective twist persistence length C_{eff} and buckling torque by comparing simulations and measurements (Fig. 4d). To characterize the braiding geometry in the measurements, we estimated $a \cdot b$ and $a + b$ from the measured hat tip size and the measured hat-top slope, respectively, using the simulated

relations shown in Fig. 4b. We first examined how C_{eff} depends on these geometric parameters. Both simulations and measurements show little dependence of C_{eff} on $a \cdot b$ or $a + b$ (Fig. 4d). We then examined how the buckling torque depends on these geometric parameters. Both simulations and measurements show that the buckling torque remains essentially unchanged with either $a \cdot b$ or $a + b$ (Fig. 4d). Thus, plectoneme formation of braided DNA occurs at a critical torque, regardless of the geometry of the substrate. Consequently, when a large torque gap is present, the turns required to reach the critical buckling torque are reduced (Fig. 3; Fig. S1b,c).

Thus, both measurements and simulations show how the braiding geometry modulates torsional mechanics of braiding. These results provide further support for the conclusion that large end separations lead to larger torque gaps and torque overshoots, thereby creating a 'torsional barrier' to the initiation of braiding.

Discussion

Our work demonstrates that DNA braiding geometry plays a crucial role in the torsional mechanics of DNA braiding. These findings have significant implications for DNA supercoiling partitioning and the torsional resistance experienced by the replisome. During replication, DNA supercoiling generated by replication must be distributed either ahead of or behind the replisome. Supercoiling partitioning behind the replisome will lead to fork rotation and intertwine (braid) the two daughter DNA molecules and must be untangled by topoisomerases before chromosome segregation. Our work allows prediction of this supercoiling partitioning and the accompanying torsional stress.

For simplicity, we consider a case where DNA replication takes place over a naked DNA and proceeds to the middle of the DNA substrate. Since the daughter strands are brought together at one end by the replisome and at the other end by SMC proteins or another replisome, the braiding geometry resembles the 'O substrate' (Fig. 5a). If topoisomerase activity nearly keeps up with replication, the DNA superhelical density is low. Since the torsional stiffness of braided DNA is much smaller than that of a single DNA molecule, replication will lead to fork rotation, and the supercoiling will partition predominantly behind the replisome.

Thus, although the small end separations help alleviate some torsional stress, they will also lead to daughter DNA intertwining. If topoisomerase activity cannot keep up with replication, the DNA superhelical density may increase, leading to buckling of the parental single-DNA strand at the front and limiting further accumulation of torsional stress. Concurrently, the fork stops rotating, and additional supercoiling will partition to the front of the replisome.

In contrast, if the daughter strands are brought together at one end by the replisome but fail to be brought together at the other end by SMC proteins, then the braiding geometry resembles the 'V substrate' (Fig. 5b). This geometry will result in a torque gap, which imposes a 'torsional barrier' to braiding initiation. Consider a case when topoisomerase activity nearly keeps up with replication, so that the DNA superhelical density is low. The fork will not rotate due to the 'torsional barrier', and supercoiling will be directed predominantly to the front of the replisome. Although the two daughter DNA molecules are minimally intertwined, the replisome experiences a greater torsional stress. Interestingly, previous studies show that DNA intertwining is reduced upon inactivation of cohesin (*66*) and the progression of the replication fork is slowed in cohesion-deficient cells (*67*), providing possible evidence for our proposed model. If topoisomerase activity cannot keep up with replication, an increase in superhelical density will braid the daughter strands and subsequently buckle the single DNA substrate in the front. Once buckling occurs, torque ceases to increase, and the fork stops rotating. Any additional supercoiling will partition to the front of the replisome.

Although the predictions of Fig. 5 are obtained for the naked DNA substrates, the framework laid out here should be general. *In vivo*, DNA is associated with bound proteins, which could significantly alter its torsional properties. Indeed, converting naked DNA to chromatin has been shown to significantly change the torsional mechanics of chromatin (*4*, *68*), which will in turn impact supercoiling partitioning. In addition, these predictions are based on results at a moderate tension of 2 pN, but overall conclusions should hold over a broad range of forces (> 0.1 pN). Our work suggests that geometry should also play a crucial role in supercoiling partitioning during replication on these protein-bound substrates.

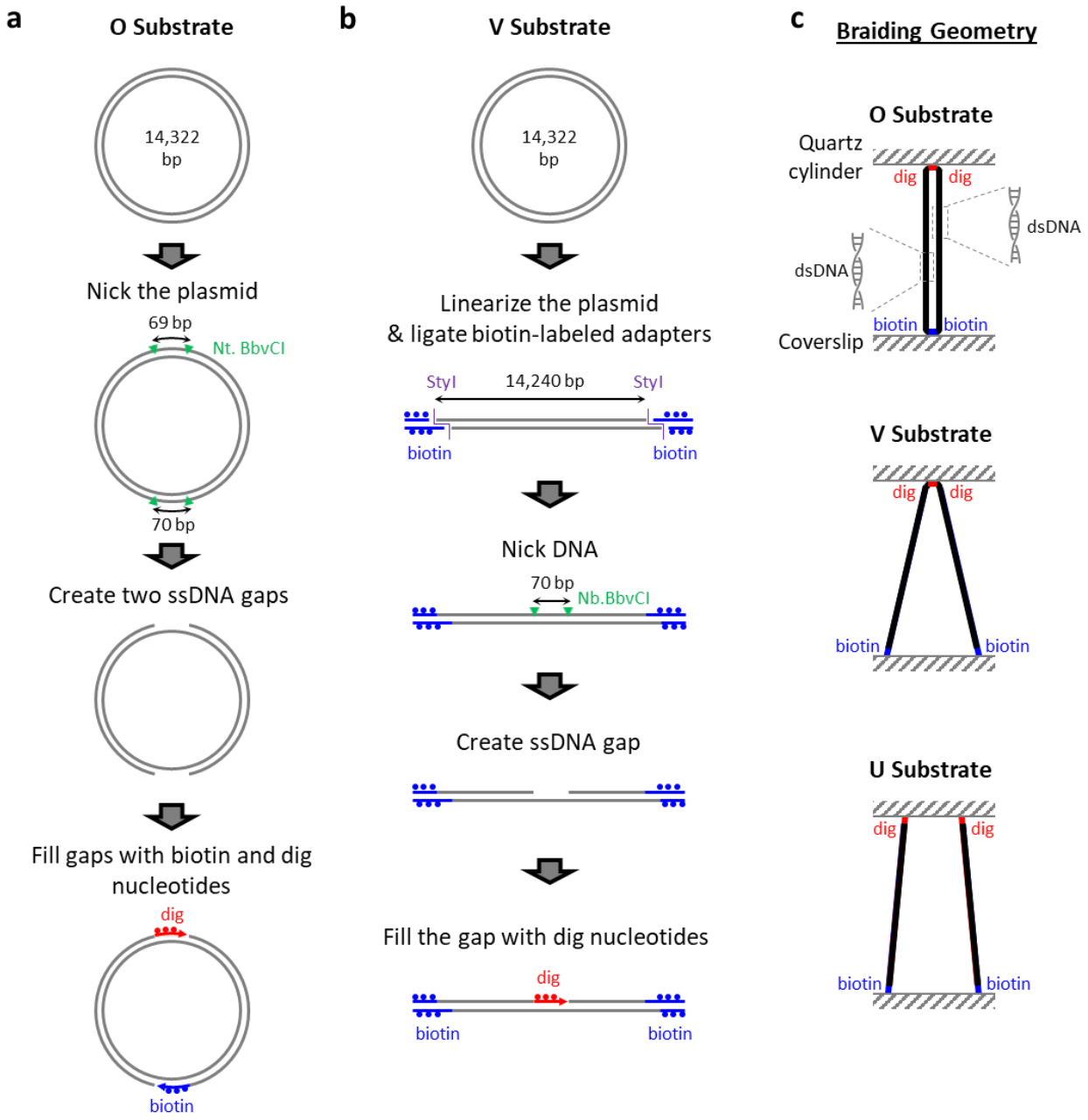

Fig. 1. Construction of braiding substrates with defined geometries.

a. 'O substrate' design and preparation. The final product has two dsDNA strands for braiding, each 7.1 kb in length, with minimal separations at both ends. The top end of the 'O substrate' is labeled with multi-digoxigenin tags (red), while the bottom end is labeled with multi-biotin tags (blue). This substrate allows end separations of the two 'daughter' DNA strands to be ~ 70 bp once the substrate is anchored between a coverslip and a quartz cylinder held in an AOT.

b. ‘V substrate’ design and preparation. The final product has two ‘daughter’ strands for braiding, each 7.1 kb in length, with a minimal separation at one end. The center of the substrate is labeled with multi-digoxigenin tags (red), resulting in an end separation ~ 70 bp. The two biotin-labeled (blue) ends allow variable end separations once anchored to a coverslip surface.

c. Three different braiding geometries, achieved by different braiding substrates. Each substrate is anchored between the coverslip surface and the bottom surface of a quartz cylinder held by the AOT.

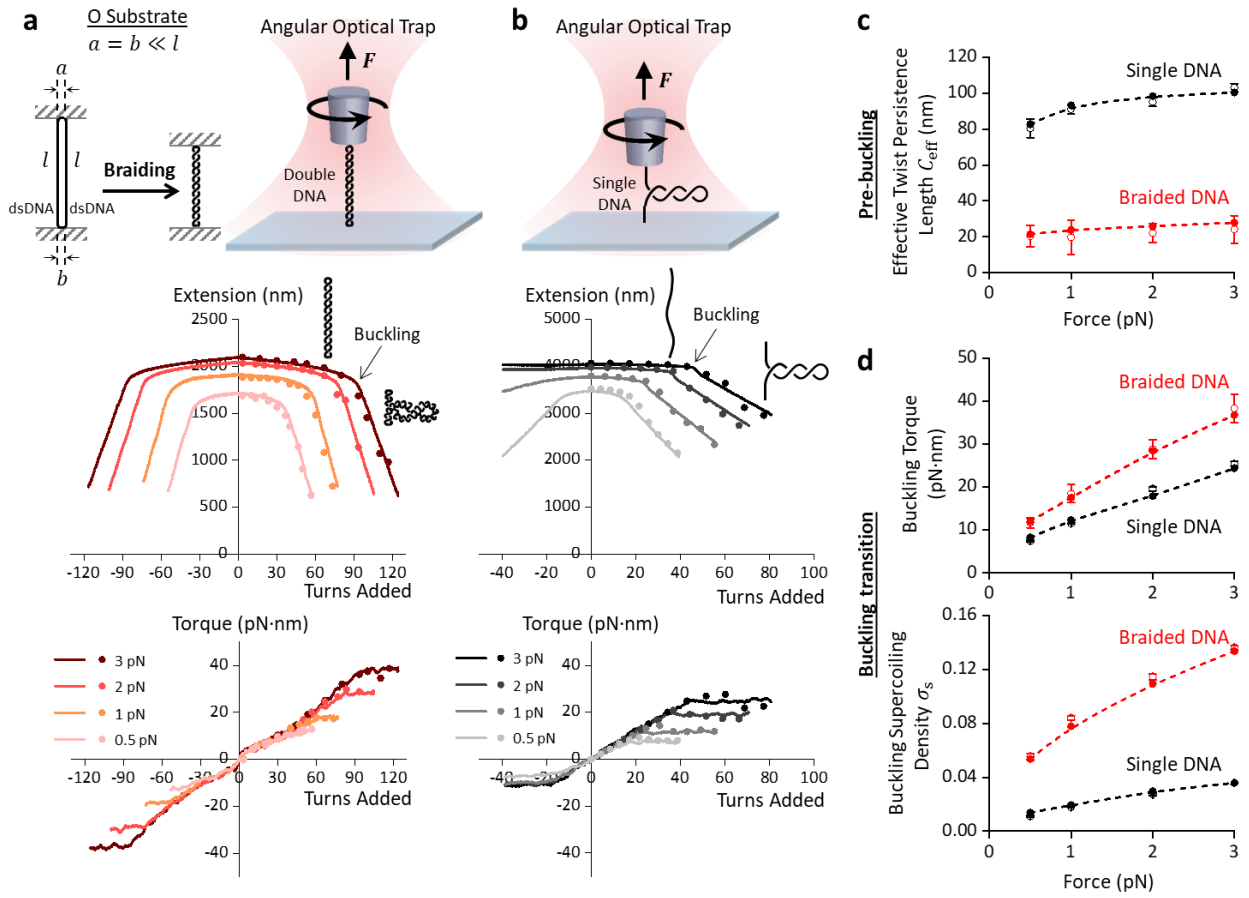

Fig. 2. Torsional mechanical properties of braiding the 'O substrate', in comparison with those of twisting a single-DNA substrate.

a. Torsional measurements of braiding the 'O substrate' using the AOT. The cartoons at the top show the experimental configuration. The 'O substrate' is torsionally constrained between the bottom surface of an optically trapped quartz cylinder and the surface of the coverslip of a sample chamber, with both anchoring lengths a and b ~ 70 bp, significantly smaller than the 'daughter' DNA length l. Both anchor segments are torsionally constrained to their anchoring surfaces. While turns are added to the substrate via cylinder rotation as the substrate is held under a constant force, extension and torque are simultaneously measured via the AOT. The bottom plots show the measured extension and torque (lines), along with a direct comparison with the MC simulation results (dots). For each force, the measurements are the means of N = 15 molecules.

b. Torsional measurements of twisting a single-DNA substrate. The cartoons at the top show the experimental configuration for twisting a single-DNA substrate using the AOT, in a way akin to that of the 'O substrate'. The single-DNA substrate is 12.7 kb in length, flanked by two end-tagged DNA segments of about 500 bp to torsionally constrain the substrate between the two surfaces (Methods). The bottom plots show the measured extension and torque (lines), along with comparison with the MC simulation results (dots). For each force, the measurements are averaged from *N* = 15-19 molecules.

c. Effective twist persistence length C_{eff} of braiding the 'O substrate' versus force. The C_{eff} is obtained from the torque-turns relation near zero turns (Methods) from both measurements (open dots with error bars being SDs) and simulations (solid dots). For comparison, also shown are the corresponding C_{eff} data of a single-DNA molecule. The dashed lines are interpolations from the simulation results to guide the eye.

d. Buckling torque and buckling superhelical density of braiding the 'O substrate' versus force. Superhelical density of braided DNA (the catenation density) is defined as Ca/Lk_0, where Ca is the catenation number and Lk_0 is the linking number of a relaxed DNA for one of the 'daughter' DNAs for braiding. Buckling torque and buckling superhelical density are determined from both measurements (open dots with error bars being SDs) and simulations (solid dots). For comparison, also shown are the buckling torque and buckling superhelical density of a single-DNA molecule (grey dots). The dashed lines are interpolations from the simulation results to guide the eye.

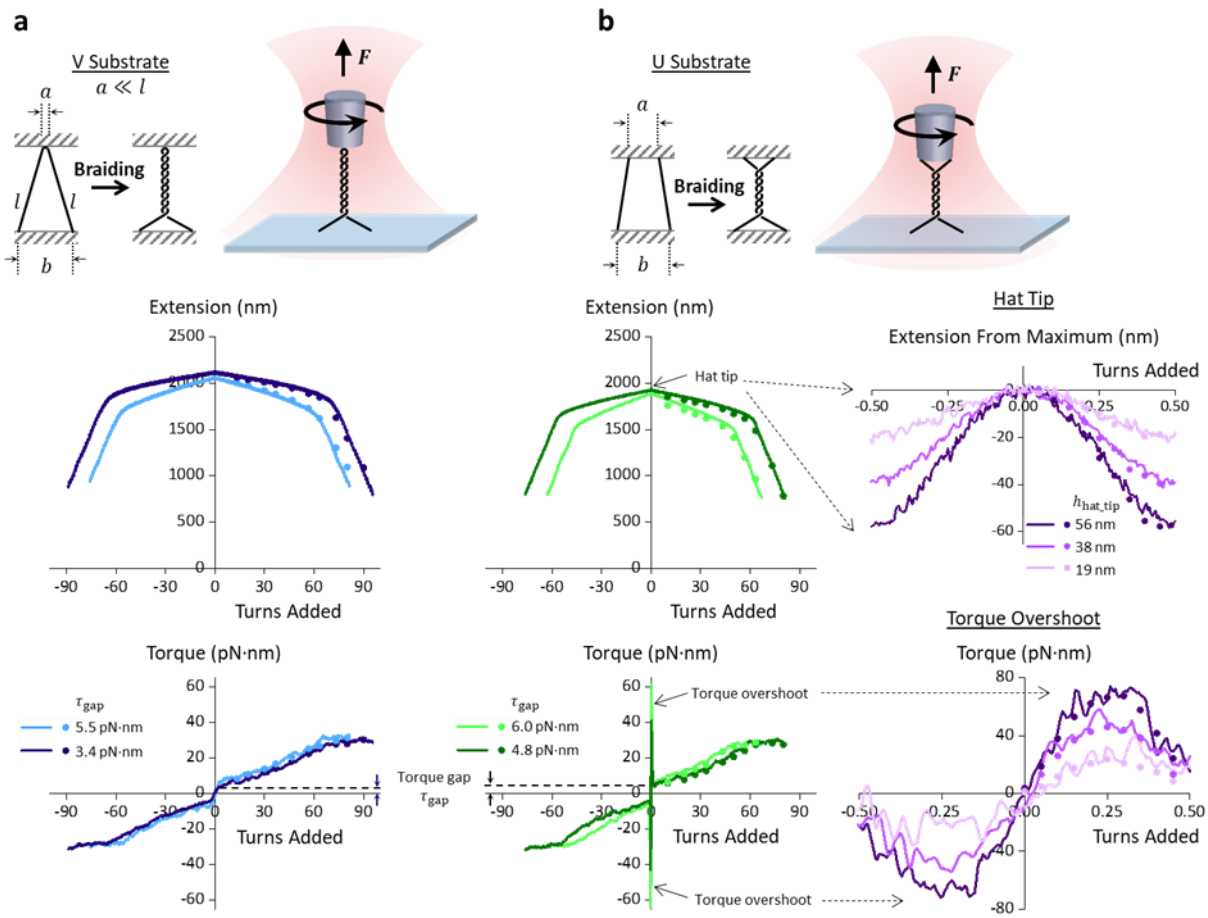

Fig. 3. Torsional measurements of braiding the 'V substrate' and the 'U substrate'.

a. Torsional measurements of braiding the 'V substrate' using the AOT. The cartoons at the top show the experimental configuration, similar to that of the 'O substrate', except that the anchor separations at the bottom end can be substantial. The 'V substrate' is held under 2 pN and torsionally constrained between the bottom surface of an optically trapped quartz cylinder and the surface of the coverslip of a sample chamber, with the top anchoring separation at the cylinder constrained to be ~ 70 bp (a = 24 nm) while the bottom anchoring separation can vary substantially. The bottom plots show the measured extension and torque during braiding of the 'V substrate' with two torque gap values (lines), along with a direct comparison with the MC simulation results (dots) with b chosen to achieve reasonable agreement with measurements. The dashed lines indicate the torque gap τ_{gap}. For τ_{gap} = 3.4 pN·nm, measurements are averaged from N = 12 molecules, and simulations are performed with b = 421 nm. For τ_{gap} =

5.5 pN·nm, measurements are averaged from *N* = 5 molecules, and simulations are performed with b = 850 nm.

b. Torsional measurements of braiding the 'U substrate' using the AOT. The cartoons at the top show the experimental configuration, similar to that of the 'O substrate' and 'V substrate, except that the anchor separations at both ends can vary substantially. The two plots on the left show the measured extension and torque during braiding of the 'U substrate' with two torque gap values (lines): τ_{gap}= 4.8 pN·nm, *N* = 7; τ_{gap}= 6.0 pN·nm, *N* = 11. These plots are directly compared with MC simulation results (dots) with a and b chosen to achieve reasonable agreement with measurements: assuming $a\ (= b)$ = 270 nm and 543 nm respectively. The two plots on the right show the measured extension and torque within the first ±0.5 turns of braiding of the 'U substrate'. For these plots, traces are classified based on their hat tip size: 19 nm (*N* = 13), 38 nm (*N* = 18), 56 nm (*N* = 9). These plots are directly compared with MC simulation results (dots) with a and b chosen to achieve reasonable agreement with measurements: $a\ (= b) =$ 288 nm, 408 nm, and 500 nm, respectively.

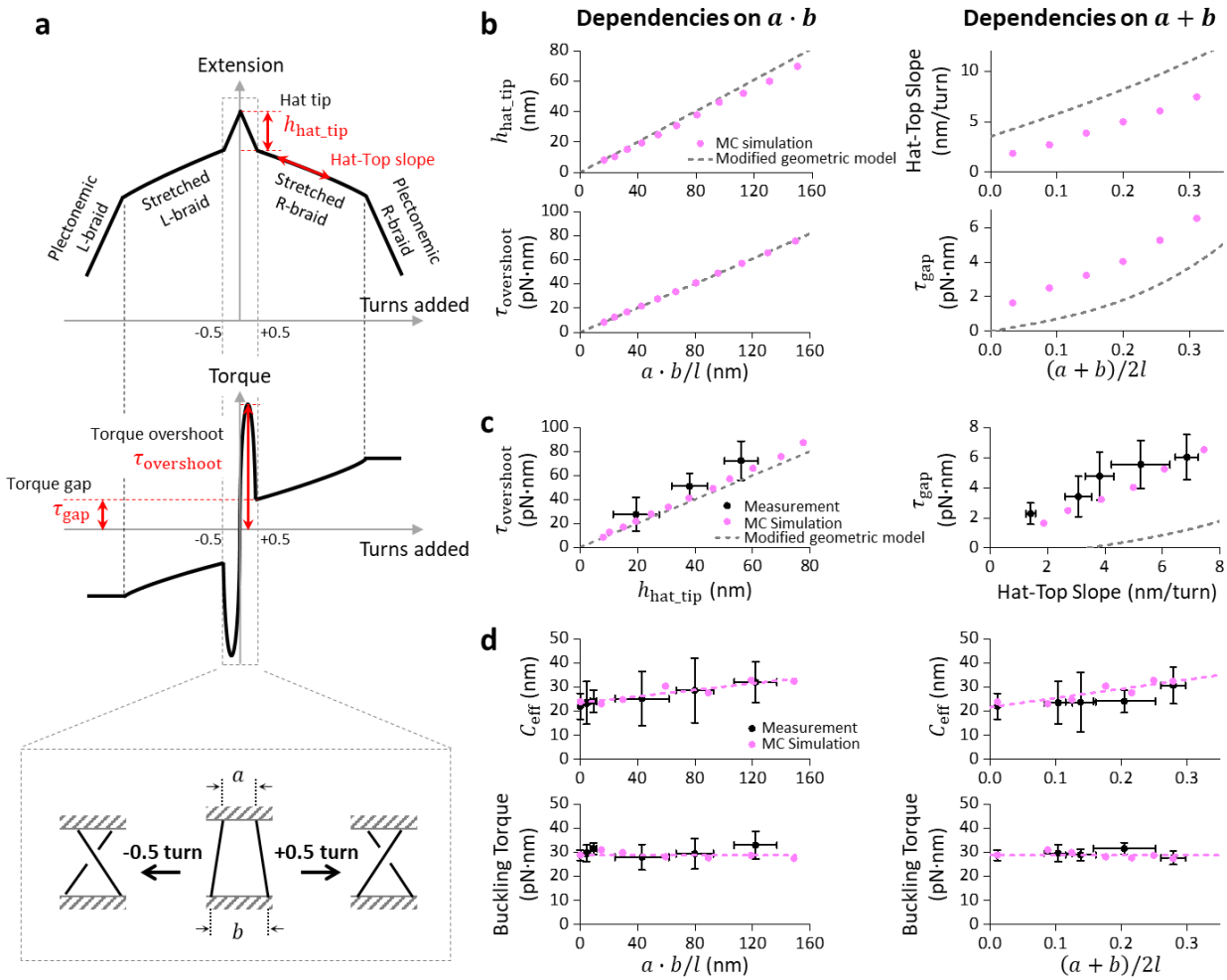

Fig. 4. Braiding geometry governs the torsional properties of DNA braiding.

a. A sketch depicting torsional responses of a double-DNA held at a constant force. We consider a general condition in which both a and b are substantial. From 0 to ±0.5 turns (cartoons shown at the bottom), the extension-turns relation (also called the hat curve) shows a sharp decrease in extension. Concurrently, the torque-turns relation shows dramatic, sinusoidal-like torque spikes, peaking at ±0.25 turns. We defined the extension drop as $h_{\mathrm{hat_tip}}$ and the amplitude of the sinusoidal-like torque profile as $\tau_{\mathrm{overshoot}}$. At ±0.5 turns, the two DNA strands are first brought into contact with each other, initiated braiding with a nonzero torque, which we defined as τ_{gap}. As more turns are introduced, the two DNA strands intertwine, leading to a near-linear extension slope, which we refer to as the hat-top slope, followed by the buckling of braided DNA and formation of a plectoneme.

b. MC simulations of dependencies of $h_{\text{hat_tip}}$, $\tau_{\text{overshoot}}$, hat-top slope magnitude, and τ_{gap} on braiding geometry at 2 pN. The two plots on the left show how $h_{\text{hat_tip}}$ and $\tau_{\text{overshoot}}$ depend on $a \cdot b$, while the two plots on the right show how the hat-top slope magnitude and τ_{gap} depend on $a + b$. For comparison, the predictions from the modified geometric model (Methods) are also shown.

c. Experimental validation of the MC simulations shown in **b**. To directly compare the simulation results with measurements, we plot the measured $\tau_{\text{overshoot}}$ versus $h_{\text{hat_tip}}$ and the measured τ_{gap} versus the hat-top slope magnitude using data from Fig. 2 and Fig. 3 and compare with those from simulations and the geometric model.

d. Dependencies of the effective twist persistence length C_{eff} and buckling torque on braiding geometry from both measurements and simulations. The left two plots show how C_{eff} and the buckling torque depend on $a \cdot b$. Each measured data point represents an average of *N* = 5-15 traces. The right two plots show how C_{eff} and the buckling torque depend on $a + b$. Each measured data point represents an average of *N* = 5-15 traces. Error bars represent SDs. The dashed lines are linear fits to the simulation results to guide the eye.

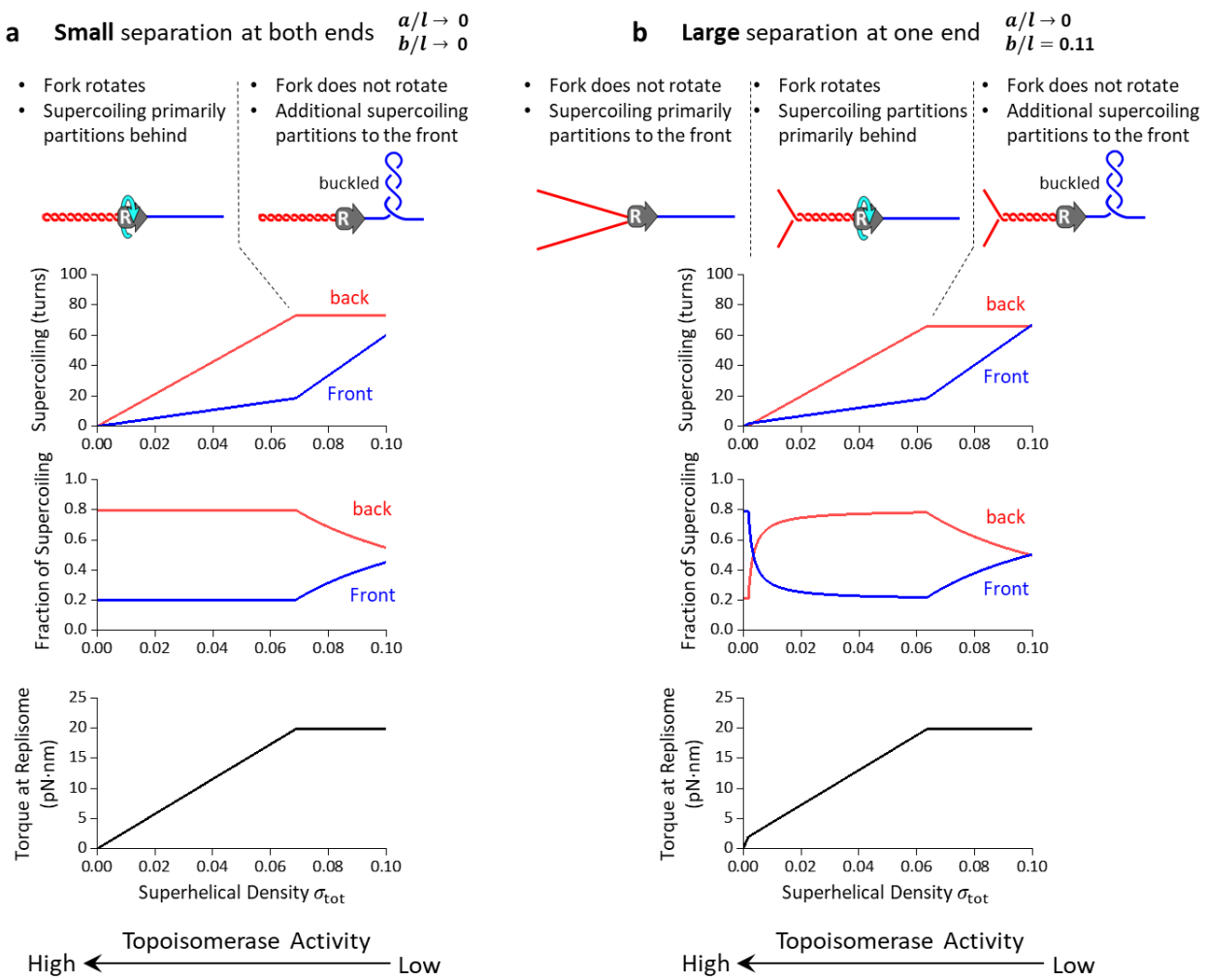

Fig. 5. Supercoiling partitioning during DNA replication altered by different substrate geometries. Shown are predictions of two example substrate geometries when the replisome has replicated to the middle of the DNA template (a total length of 14 kb). The predictions are based on the torsional mechanical measurements of a single DNA-molecule substrate (in front of the replisome) and a double-DNA molecule substrate (behind the replisome). For simplicity, the illustrative plots are obtained by considering only the linear term of torsional stiffness of the substrate at 2 pN (Table S3).

a. Daughter-strand geometry with small separation at both ends: $a/l = b/l \approx 0$. Under this geometrical configuration, there is no torsional barrier to limit supercoiling partitioning behind the replisome. If topoisomerase activity is high, the superhelical density is low. Under this

condition, significant fork rotation can occur. The intertwining of the daughter strands prevents chromosome segregation but buffers torsional resistance to replisome progression. If topoisomerase activity is reduced, the superhelical density increases, and so does the torque at the replisome. This eventually leads to the single-DNA substrate at the front buckling to form a plectoneme, which is highly effective at limiting torsional stress accumulation. Once buckling occurs, the fork stops rotating, leading to additional supercoiling partitioning only to the front.

b. Daughter-strand geometry with a large separation distal to the replisome: $a/l \approx 0$ and b/l = 0.11. This may occur when SMC proteins fail to bring the two daughter strands together at the end distal to the replisome. Under this geometrical configuration, braiding the daughter strands must first overcome a 'torsional barrier' presented by the torque gap that resists the initiation of braiding. If topoisomerase activity is low and the replisome overcomes this barrier, the fork rotates, and supercoiling partitions preferentially behind the replisome. This continues until the single-DNA substrate in the front buckles, limiting the torsional stress accumulation. Once buckling occurs, the fork stops rotation, and additional supercoiling will be partitioned only to the front of the replisome.

Author Contributions

S.P. and M.D.W conceived the design of the braiding substrates. S.P. created the original template plasmid. Y.H. and S.P. prepared the braiding substrates. Y.H. fabricated the quartz cylinders. Y.H. designed and optimized the single-molecule assays. Y.H. performed measurements with assistance from H.W.. Y.H. performed data analysis. G.S performed the MC simulations with assistance from H.W.. H.W. modified the geometric model for DNA braiding. Y.H. and M.D.W. drafted the manuscript with revisions by all authors. M.D.W. supervised the project.

Acknowledgments

We thank members of the Wang Laboratory for helpful discussions, Dr. J. T. Inman for providing technical assistance in updating the AOT software, Drs. J. Lee and X. Gao for the preliminary exploration of this project, Dr. X. Jia for the helpful discussion on DNA-substrate preparation and for providing the 6.5 kb torsionally unconstrained DNA used in this work, and Dr. M. Wu for providing the 12.7 kb torsionally constrained DNA. This work is supported by the National Institutes of Health grant R01GM136894 (to M.D.W.). M.D.W. is a Howard Hughes Medical Institute investigator. This work was performed in part at the Cornell NanoScale Facility, a member of the National Nanotechnology Coordinated Infrastructure (NNCI), which is supported by the National Science Foundation (Grant NNCI-2025233).

Competing interests: The authors declare that they have no competing interests.

Data and materials availability: All data needed to evaluate the conclusions in the paper are present in the paper and/or the Supplementary Materials.

References

1. L. Postow, N. J. Crisona, B. J. Peter, C. D. Hardy, N. R. Cozzarelli, Topological challenges to DNA replication: Conformations at the fork. *Proc. Natl. Acad. Sci.* **98**, 8219–8226 (2001).

2. C. J. Ullsperger, A. V. Vologodskii, N. R. Cozzarelli, "Unlinking of DNA by Topoisomerases During DNA Replication" in *Nucleic Acids and Molecular Biology*, F. Eckstein, D. M. J. Lilley, Eds. (Springer Berlin Heidelberg, Berlin, Heidelberg, 1995), pp. 115–142.

3. A. Keszthelyi, N. E. Minchell, J. Baxter, The Causes and Consequences of Topological Stress during DNA Replication. *Genes* **7**, 134 (2016).

4. T. T. Le, X. Gao, S. H. Park, J. Lee, J. T. Inman, J. H. Lee, J. L. Killian, R. P. Badman, J. M. Berger, M. D. Wang, Synergistic Coordination of Chromatin Torsional Mechanics and Topoisomerase Activity. *Cell* **179**, 619-631.e15 (2019).

5. X. Jia, X. Gao, S. Zhang, J. T. Inman, Y. Hong, A. Singh, F. Rashid, J. M. Berger, S. S. Patel, M. D. Wang, Torsion is a dynamic regulator of DNA replication stalling and reactivation. *Nat. Commun.* **16**, 10543 (2025).

6. J. Cebrián, A. Castán, V. Martínez, M. J. Kadomatsu-Hermosa, C. Parra, M. J. Fernández-Nestosa, C. Schaerer, P. Hernández, D. B. Krimer, J. B. Schvartzman, Direct Evidence for the Formation of Precatenanes during DNA Replication*. *J. Biol. Chem.* **290**, 13725–13735 (2015).

7. B. J. Peter, C. Ullsperger, H. Hiasa, K. J. Marians, N. R. Cozzarelli, The Structure of Supercoiled Intermediates in DNA Replication. *Cell* **94**, 819–827 (1998).

8. M. M. Seidman, N. P. Salzman, Late replicative intermediates are accumulated during simian virus 40 DNA replication in vivo and in vitro. *J. Virol.* **30**, 600–609 (1979).

9. O. Sundin, A. Varshavsky, Arrest of segregation leads to accumulation of highly intertwined catenated dimers: Dissection of the final stages of SV40 DNA replication. *Cell* **25**, 659–669 (1981).

10. D. P. Tapper, M. L. DePamphilis, Discontinuous DNA replication: Accumulation of simian virus 40 DNA at specific stages in its replication. *J. Mol. Biol.* **120**, 401–422 (1978).

11. S. A. Schalbetter, S. Mansoubi, A. L. Chambers, J. A. Downs, J. Baxter, Fork rotation and DNA precatenation are restricted during DNA replication to prevent chromosomal instability. *Proc. Natl. Acad. Sci.* **112**, E4565–E4570 (2015).

12. T. M. Retzer, L. T. Rajappa, M. Takahashi, S. M. Hamdan, K. E. Duderstadt, Real-time imaging of rotation during synthesis by the replisome. *bioRxiv*, 2025–04 (2025).

13. L. V. Campos, S. X. Van Ravenstein, E. J. Vontalge, B. H. Greer, D. R. Heintzman, T. Kavlashvili, W. H. McDonald, K. L. Rose, B. F. Eichman, J. M. Dewar, RTEL1 and MCM10 overcome topological stress during vertebrate replication termination. *Cell Rep.* **42**, 112109 (2023).

14. Y. Pommier, A. Nussenzweig, S. Takeda, C. Austin, Human topoisomerases and their roles in genome stability and organization. *Nat. Rev. Mol. Cell Biol.* **23**, 407–427 (2022).

15. J. J. Champoux, DNA topoisomerases: structure, function, and mechanism. *Annu. Rev. Biochem.* **70**, 369–413 (2001).

16. M. Stracy, A. J. M. Wollman, E. Kaja, J. Gapinski, J.-E. Lee, V. A. Leek, S. J. McKie, L. A. Mitchenall, A. Maxwell, D. J. Sherratt, M. C. Leake, P. Zawadzki, Single-molecule imaging of DNA gyrase activity in living Escherichia coli. *Nucleic Acids Res.* **47**, 210–220 (2019).

17. F. Kouzine, S. Sanford, Z. Elisha-Feil, D. Levens, The functional response of upstream DNA to dynamic supercoiling in vivo. *Nat. Struct. Mol. Biol.* **15**, 146–154 (2008).

18. F. Kouzine, A. Gupta, L. Baranello, D. Wojtowicz, K. Ben-Aissa, J. Liu, T. M. Przytycka, D. Levens, Transcription-dependent dynamic supercoiling is a short-range genomic force. *Nat. Struct. Mol. Biol.* **20**, 396–403 (2013).

19. C. Naughton, N. Avlonitis, S. Corless, J. G. Prendergast, I. K. Mati, P. P. Eijk, S. L. Cockroft, M. Bradley, B. Ylstra, N. Gilbert, Transcription forms and remodels supercoiling domains unfolding large-scale chromatin structures. *Nat. Struct. Mol. Biol.* **20**, 387–395 (2013).

20. S. S. Teves, S. Henikoff, Transcription-generated torsional stress destabilizes nucleosomes. *Nat. Struct. Mol. Biol.* **21**, 88–94 (2014).

21. S. Chong, C. Chen, H. Ge, X. S. Xie, Mechanism of Transcriptional Bursting in Bacteria. *Cell* **158**, 314–326 (2014).

22. K. S. Lang, A. N. Hall, C. N. Merrikh, M. Ragheb, H. Tabakh, A. J. Pollock, J. J. Woodward, J. E. Dreifus, H. Merrikh, Replication-Transcription Conflicts Generate R-Loops that Orchestrate Bacterial Stress Survival and Pathogenesis. *Cell* **170**, 787-799.e18 (2017).

23. D. Racko, F. Benedetti, J. Dorier, A. Stasiak, Are TADs supercoiled? *Nucleic Acids Res.* **47**, 521–532 (2019).

24. L. Postow, C. Ullsperger, R. W. Keller, C. Bustamante, A. V. Vologodskii, N. R. Cozzarelli, Positive Torsional Strain Causes the Formation of a Four-way Junction at Replication Forks*. *J. Biol. Chem.* **276**, 2790–2796 (2001).

25. M. S. Guo, D. L. Haakonsen, W. Zeng, M. A. Schumacher, M. T. Laub, A Bacterial Chromosome Structuring Protein Binds Overtwisted DNA to Stimulate Type II Topoisomerases and Enable DNA Replication. *Cell* **175**, 583-597.e23 (2018).

26. G. Charvin, A. Vologodskii, D. Bensimon, V. Croquette, Braiding DNA: Experiments, Simulations, and Models. *Biophys. J.* **88**, 4124–4136 (2005).

27. S. Brahmachari, J. F. Marko, Torque and buckling in stretched intertwined double-helix DNAs. *Phys. Rev. E* **95**, 052401 (2017).

28. Y. Gao, Y. Cui, T. Fox, S. Lin, H. Wang, N. de Val, Z. H. Zhou, W. Yang, Structures and operating principles of the replisome. *Science* **363**, eaav7003 (2019).

29. Y. Murayama, C. P. Samora, Y. Kurokawa, H. Iwasaki, F. Uhlmann, Establishment of DNA-DNA Interactions by the Cohesin Ring. *Cell* **172**, 465-477.e15 (2018).

30. S. A. Schalbetter, A. Goloborodko, G. Fudenberg, J.-M. Belton, C. Miles, M. Yu, J. Dekker, L. Mirny, J. Baxter, SMC complexes differentially compact mitotic chromosomes according to genomic context. *Nat. Cell Biol.* **19**, 1071–1080 (2017).

31. S. Glaser, M. I. Molodtsov, J. F. X. Diffley, F. Uhlmann, Replisome passage through the cohesin ring. *Cell* **188**, 5618-5631.e14 (2025).

32. M. D. Stone, Z. Bryant, N. J. Crisona, S. B. Smith, A. Vologodskii, C. Bustamante, N. R. Cozzarelli, Chirality sensing by *Escherichia coli* topoisomerase IV and the mechanism of type II topoisomerases. *Proc. Natl. Acad. Sci.* **100**, 8654–8659 (2003).

33. G. Charvin, D. Bensimon, V. Croquette, Single-molecule study of DNA unlinking by eukaryotic and prokaryotic type-II topoisomerases. *Proc. Natl. Acad. Sci.* **100**, 9820–9825 (2003).

34. K. C. Neuman, G. Charvin, D. Bensimon, V. Croquette, Mechanisms of chiral discrimination by topoisomerase IV. *Proc. Natl. Acad. Sci.* **106**, 6986–6991 (2009).

35. B. Xiao, S. Brahmachari, Y. Liu, K. Ding, J. F. Marko, Measurement of the torque in braided DNAs using a thermodynamic Maxwell relation. *bioRxiv*, 2020.02.07.938209 (2020).

36. H. Bai, M. Sun, P. Ghosh, G. F. Hatfull, N. D. F. Grindley, J. F. Marko, Single-molecule analysis reveals the molecular bearing mechanism of DNA strand exchange by a serine recombinase. *Proc. Natl. Acad. Sci.* **108**, 7419–7424 (2011).

37. M. Nöllmann, M. D. Stone, Z. Bryant, J. Gore, N. J. Crisona, S.-C. Hong, S. Mitelheiser, A. Maxwell, C. Bustamante, N. R. Cozzarelli, Multiple modes of Escherichia coli DNA gyrase activity revealed by force and torque. *Nat. Struct. Mol. Biol.* **14**, 264–271 (2007).

38. Y. Seol, A. H. Hardin, M.-P. Strub, G. Charvin, K. C. Neuman, Comparison of DNA decatenation by Escherichia coli topoisomerase IV and topoisomerase III: implications for non-equilibrium topology simplification. *Nucleic Acids Res.* **41**, 4640–4649 (2013).

39. K. Terekhova, J. F. Marko, A. Mondragón, Single-molecule analysis uncovers the difference between the kinetics of DNA decatenation by bacterial topoisomerases I and III. *Nucleic Acids Res.* **42**, 11657–11667 (2014).

40. Carlos J. Martínez-Santiago, E. Quiñones, Torque measurements during the spontaneous unbraiding of DNA molecules in the absence of pulling forces. *Chem. Phys.* **491**, 25–32 (2017).

41. C. J. Martínez-Santiago, E. Quiñones, On matching the magnetic torque exerted by a rotating magnetic field to the torsional stiffness of braided DNA molecules for torque estimations. *Chem. Phys.* **519**, 74–84 (2019).

42. S. J. McKie, P. R. Desai, Y. Seol, A. M. B. Allen, A. Maxwell, K. C. Neuman, Topoisomerase VI is a chirally-selective, preferential DNA decatenase. *eLife* **11**, e67021 (2022).

43. J. W. Shepherd, S. Guilbaud, Z. Zhou, J. A. L. Howard, M. Burman, C. Schaefer, A. Kerrigan, C. Steele-King, A. Noy, M. C. Leake, Correlating fluorescence microscopy, optical and magnetic tweezers to study single chiral biopolymers such as DNA. *Nat. Commun.* **15**, 2748 (2024).

44. N. A. W. Bell, P. J. Haynes, K. Brunner, T. M. de Oliveira, M. M. Flocco, B. W. Hoogenboom, J. E. Molloy, Single-molecule measurements reveal that PARP1 condenses DNA by loop stabilization. *Sci. Adv.* **7**, eabf3641 (2021).

45. S. Brahmachari, K. H. Gunn, R. D. Giuntoli, A. Mondragón, J. F. Marko, Nucleation of Multiple Buckled Structures in Intertwined DNA Double Helices. *Phys. Rev. Lett.* **119**, 188103 (2017).

46. K. Yogo, T. Ogawa, M. Hayashi, Y. Harada, T. Nishizaka, K. Kinosita, Direct Observation of Strand Passage by DNA-Topoisomerase and Its Limited Processivity. *PLOS ONE* **7**, e34920 (2012).

47. M. C. Noom, B. van den Broek, J. van Mameren, G. J. L. Wuite, Visualizing single DNA-bound proteins using DNA as a scanning probe. *Nat. Methods* **4**, 1031–1036 (2007).

48. Md. T. Hoque, F. Ishikawa, Cohesin Defects Lead to Premature Sister Chromatid Separation, Kinetochore Dysfunction, and Spindle-assembly Checkpoint Activation*. *J. Biol. Chem.* **277**, 42306–42314 (2002).

49. Y. Hong, F. Ye, X. Gao, J. T. Inman, M. D. Wang, Tunable elliptical cylinders for rotational mechanical studies of single DNA molecules. *Sci. Adv.* **10**, eadr4519.

50. C. Deufel, S. Forth, C. R. Simmons, S. Dejgosha, M. D. Wang, Nanofabricated quartz cylinders for angular trapping: DNA supercoiling torque detection. *Nat. Methods* **4**, 223–225 (2007).

51. Y. Hong, F. Ye, J. Qian, X. Gao, J. T. Inman, M. D. Wang, Optical torque calculations and measurements for DNA torsional studies. *Biophys. J.*, doi: 10.1016/j.bpj.2024.07.005 (2024).

52. J. Lee, M. Wu, J. T. Inman, G. Singh, S. H. Park, J. H. Lee, R. M. Fulbright, Y. Hong, J. Jeong, J. M. Berger, M. D. Wang, Chromatinization modulates topoisomerase II processivity. *Nat Commun* **14**, 6844 (2023).

53. X. Gao, J. T. Inman, M. D. Wang, Angular Optical Trapping to Directly Measure DNA Torsional Mechanics. *Methods Mol Biol* **2478**, 37–73 (2022).

54. X. Gao, Y. Hong, F. Ye, J. T. Inman, M. D. Wang, Torsional Stiffness of Extended and Plectonemic DNA. *Phys. Rev. Lett.* **127**, 028101 (2021).

55. J. Ma, C. Tan, X. Gao, R. M. Fulbright, J. W. Roberts, M. D. Wang, Transcription factor regulation of RNA polymerase's torque generation capacity. *Proc Natl Acad Sci U A* **116**, 2583–2588 (2019).

56. J. Ma, L. Bai, M. D. Wang, Transcription Under Torsion. *Science* **340**, 1580–1583 (2013).

57. S. Forth, C. Deufel, M. Y. Sheinin, B. Daniels, J. P. Sethna, M. D. Wang, Abrupt buckling transition observed during the plectoneme formation of individual DNA molecules. *Phys. Rev. Lett.* **100** (2008).

58. B. C. Daniels, S. Forth, M. Y. Sheinin, M. D. Wang, J. P. Sethna, Discontinuities at the DNA supercoiling transition. *Phys. Rev. E* **80** (2009).

59. M. Y. Sheinin, S. Forth, J. F. Marko, M. D. Wang, Underwound DNA under Tension: Structure, Elasticity, and Sequence-Dependent Behaviors. *Phys. Rev. Lett.* **107**, 108102 (2011).

60. D. J. Lee, R. Cortini, A. P. Korte, E. L. Starostin, G. H. M. van der Heijden, A. A. Kornyshev, Chiral effects in dual-DNA braiding. *Soft Matter* **9**, 9833–9848 (2013).

61. R. Cortini, A. A. Kornyshev, D. J. Lee, S. Leikin, Electrostatic Braiding and Homologous Pairing of DNA Double Helices. *Biophys. J.* **101**, 875–884 (2011).

62. Y. Timsit, P. Várnai, Helical Chirality: a Link between Local Interactions and Global Topology in DNA. *PLOS ONE* **5**, e9326 (2010).

63. R. Cortini, D. J. Lee, A. Kornyshev, Chiral electrostatics breaks the mirror symmetry of DNA supercoiling. *J. Phys. Condens. Matter* **24**, 162203 (2012).

64. D. J. Lee, A. Wynveen, A. A. Kornyshev, S. Leikin, Undulations Enhance the Effect of Helical Structure on DNA Interactions. *J. Phys. Chem. B* **114**, 11668–11680 (2010).

65. A. Vologodskii, V. V. Rybenkov, Simulation of DNA catenanes. *Phys. Chem. Chem. Phys.* **11**, 10543–10552 (2009).

66. N. E. Minchell, A. Keszthelyi, J. Baxter, Cohesin Causes Replicative DNA Damage by Trapping DNA Topological Stress. *Mol. Cell* **78**, 739-751.e8 (2020).

67. M.-E. Terret, R. Sherwood, S. Rahman, J. Qin, P. V. Jallepalli, Cohesin acetylation speeds the replication fork. *Nature* **462**, 231–234 (2009).

68. J. Qian, L. Lubkowska, S. Zhang, C. Tan, Y. Hong, R. M. Fulbright, J. T. Inman, T. M. Kay, J. Jeong, D. Gotte, J. M. Berger, M. Kashlev, M. D. Wang, Chromatin Buffers Torsional Stress During Transcription. *bioRxiv*, 2024.10.15.618270 (2024).